Synergistic effects of temperature and polarization on Cr poisoning of $La_{0.6}Sr_{0.4}Co_{0.2}Fe_{0.8}O_{3-\delta}$ Solid Oxide Fuel Cell Cathodes

Na Ni, *#ab Cheng Cheng Wang,c# San Ping Jiangd and Stephen J. Skinnerb

[a] Key Lab of Education Ministry for Power Machinery and Engineering, School of Mechanical Engineering, Shanghai Jiao Tong University, Shanghai, China

[b] Department of Materials, Imperial College London, Exhibition Road, SW7 2AZ, London, U.K.

[c] Shen Zhen Polytechnic, Shenzhen, 518055, China

[d] Fuels and Energy Technology Institute & Department of Chemical Engineering, Curtin University, Perth, WA 6102, Australia

* Corresponding author. Email: na.ni@sjtu.edu.cn

# Both authors contributed equally to this work.

* Corresponding author: na.ni@sjtu.edu.cn

Abstract:

$La_{0.6}Sr_{0.4}Co_{0.2}Fe_{0.8}O_{3-\delta}$ (LSCF) solid oxide fuel cell cathodes were poisoned by Cr at different temperatures and polarization conditions with a Cr-Fe alloy as the interconnect. Cr induced degradation was analysed by electrochemical impedance spectroscopy (EIS) focusing on the electrochemical resistance (R_{chem}) that reflects the cathode electrochemical properties. It was found that R_{chem} increased more with increasing temperatures. However cathodic polarization exhibited a synergistic effect with the temperature, which accelerated the LSCF cathode degradation at 800 °C while lowered the degree of degradation at 900°C. By correlating complementary micro- and nano-scale microstructure characterization with the impedance analysis, the degradation mechanisms were investigated. A new Cr incorporation mechanism involving preferential formation of nanometre size Fe-Co-Cr-O spinel particles within the cathode up to the cathode/electrolyte interface was found to be responsible for the reduced degradation at 900 °C combined with cathodic polarization. The new mechanism reveals that the activity of B site elements in LSCF and possibly other perovskite cathodes plays an important role under certain combined temperature and polarization conditions, therefore future research in designing Cr resistant perovskite cathode materials may consider strategies that utilize the exsolution of B site elements for the formation of beneficial spinel phases.

Keywords:

Solid oxide fuel cell, Cathode, Cr poisoning, Oxygen Reduction, Nanostructure

1. Introduction

Solid oxide fuel cells (SOFCs) have received significant attention due to the ease with which they convert the chemical energy contained in fuels into electricity through electrochemical reactions. However, the commercialization of SOFCs is greatly limited by cost and durability issues. Among many cathode materials, $La_{0.6}Sr_{0.4}Co_{0.2}Fe_{0.8}O_{3-\delta}$ (LSCF) is one of the most extensively studied cathodes for intermediate temperature SOFCs, which is due to its excellent mixed electronic and ionic conductivities (MIEC), as well as high electrochemical activity for the oxygen reduction reaction at 600-800 °C [1-3]. It is well known that the durability of LSCF cathodes is not only related to Sr/Co segregation on the surface of the cathode [4-6] but also to poisoning by contaminant species including chromium, sulphur and silica and so on [3, 7, 8]. Among all contaminants mentioned above, deposition of chromium and its resulting poisoning is the main issue for cathode degradation and has been a subject of extensive investigation [5, 9, 10].

One of the most commonly investigated mechanisms of chromium deposition and poisoning of LSCF cathodes is related to the deposition of Cr species preferentially on the surface of LSCF through the formation of $SrCrO_4$ as well as Cr_2O_3 with poor electrical conductivity, which degraded cell performance by blocking the LSCF electrode layer pores [11-14]. We revealed that significant degradation of LSCF cathodes can happen before the above mentioned microscale change and is fundamentally associated with subtle nanoscale changes that occur within the cathode, such as grain boundary segregation of Cr, enhanced B-site element exsolution (both Fe and Co), and reduction of the Fe valence, with the latter two being related to Cr substitution in LSCF [15].

In the study of Cr poisoning, effects of temperature and cathodic polarization are often examined to aid in the understanding of poisoning mechanisms. Many studies have been carried out on $La_{0.65}Sr_{0.3}MnO_3$ (LSM), which is the conventional cathode material used in high temperature cells with a predominantly electronic conductivity. In terms of temperature effects, Jiang et al reported that Cr deposition at open cell voltage only occurred when temperature was as high as 1100 ^oC [16]. On the other hand, under polarization Krumpelt et al found that the cathode degraded much more at 700 ^oC than at 800 ^oC although the quantity of Cr deposited was similar at both temperatures [17]. Taniguchi et al reported similarly that between 850 to 1100 ^oC the operating cell was inferior at lower temperatures, and identified that while overall Cr deposition increased with increasing temperature, the higher cell degradation was related to more Cr deposition at the cathode/electrolyte interface at lower temperatures [18]. Cr poisoning of LSM cathodes was also found to increase with the presence of current passage and increasing current density [16, 19, 20]. Two main theories exist for the mechanisms of Cr deposition on LSM. In one, Cr deposition is considered to be a pure chemical reaction through the formation of Cr-Mn-O nuclei which then transform to Cr_2O_3 and $(Cr,Mn)_3O_4$, and the temperature and polarization effect was explained by the enhanced formation and diffusion of the nuclei at high temperatures or under polarization [16]. In the other, Cr poisoning is regarded as a result of direct electrochemical reduction of Cr (VI) gaseous specious such as CrO_3 and $Cr(OH)_2O_2$ at the triple phase boundary (TPB), and the more severe poisoning at higher current density was proposed to be a kinetic effect leading to faster Cr (VI) reduction and deposition [20].

In comparison, the study on temperature and polarization effect on the Cr deposition behaviour and resulting poisoning effects of LSCF cathodes, which show MIEC, remains limited and the related mechanisms are unclear. Under the open circuit condition, Wang et al. studied the Cr deposition on LSCF bar samples over the temperature range of 700 to 900 ^oC and found that SrO segregation decreased with decrease in temperature [21]. Under cathodic polarization of 200 mA cm^{-2}, the surface Cr deposits formed at 800°C were smaller in size and much lower in quantity in comparison to those at 900°C [12]. In terms of the polarization effect, the limited results reported in the open literature are inconsistent. By examining the distribution and phase of the Cr deposits at the LSCF external surface, Jiang et al concluded that the deposition of Cr species at the external surface of a LSCF cathode was more

pronounced in the absence of polarization than that in the presence of polarization at 900 ^{o}C [22]. Chen et al similarly found that Cr deposition at the cathode/electrolyte interface was reduced with cathodic polarization for a thin film LSCF cathode[23]. Bentzen et al reported a minor effect of the current load on the chromium poisoning of a LSCF/CGO composite cathode [24]. Konysheva et al found a complicated correlation between the amount of the Cr containing phase and the performance of the cathode as a function of the current passing [25]. The overall Cr content was highest at 0.2 A cm^{-2} in the current density range of zero and 0.5 A cm^{-2}, while the degradation was fastest under OCV, however increased with the current density when the polarization was applied.

Until now there appeared to be no systematic studies on the combined effect of temperature and polarization on firstly the Cr incorporation modes and then the resulting poisoning effects for LSCF cathodes. Furthermore, for a better understanding of its effect on the cathode degradation the Cr deposition needs to be examined across the cathode at multi-length scales, since many studies have suggested that total amount of Cr deposits at the LSCF cathode *surface* does not always correspond to the level of poisoning and our previous work revealed that *nanoscale modification inside the cathode* was the main reason for the degraded cathode performance [15]. In this paper, the fundamental understanding of the effect of temperature as well as polarization on Cr interaction with LSCF related to its poisoning was investigated. The results showed that temperature and polarization has a synergistic effect on the Cr poisoning of LSCF cathodes, which is rooted in the different nanoscale Cr incorporation mechanisms.

2. Experimental

2.1 Cell preparation

Electrolyte pellets were prepared by die pressing $Gd_{0.1}Ce_{0.9}O_{1.95}$(CGO, Fuel Cell Materials, USA) powder, followed by sintering at 1450 °C for 5 h. The pellets were 0.5–0.9 mm in thickness and 20 mm in diameter. $(La_{0.6}Sr_{0.4})_{0.95}(Co_{0.2}Fe_{0.8})O_{3-\delta}$ (LSCF, Fuel Cell Materials, USA) cathode ink was painted on the centre of CGO pellets and fired at 1050 °C for 2 h. RD diffraction The thickness of the LSCF electrode coating was 20μm and the electrode area was ~0.5 cm^2. Pt counter electrode (Pt ink, Gwent Group of Companies, United Kingdom) was painted on the opposite side of the CGO electrolyte pellets and fired at 800°C. A Pt reference electrode was attached to the edge of the electrolyte. Pt mesh was placed on the surface of the LSCF cathodes as the current collector. The half cell configuration can be seen in Figure S1.

A commercial RA446 Fe-Cr alloy (23-27% Cr, 1.5% Mn, 1%Si, 0.2% C, 0.12% N and the remaining Fe; Rolled Alloy Co., Ontario, Canada) was used as the interconnect materials. The alloys were machined into coupons (12mm×12mm×4mm) with channels (1.2 mm×1.2 mm) cut on one side of the coupons. Air was directed to the channels through an alumina tube at a flow rate of 100sccm. The interconnect was directly placed onto the surface

of the electrode. The cell configuration and the arrangement of the Fe-Cr alloy interconnect can be found in Figure S1 and in ref 26. We refer to the position where a direct contact is made between the interconnect and the cathode surface as the "rib" position, while the cathode surface under the channel of the interconnect is the "channel" position.

2.2 Electrochemical characterization

Electrochemical performance of LSCF electrodes was evaluated using a Gamry Reference 3000 potentiostat in a three-electrode configuration. Polarization behaviour of the LSCF electrodes was examined in the presence of Fe-Cr alloy under a constant cathodic current density of 200 mA cm^{-2} at 800 and 900 ^{o}C for 20 h. Current passage was interrupted from time to time to collect the electrochemical impedance spectra in open circuit, which were obtained in the frequency range of 100 kHz to 0.1 Hz with a signal amplitude of 10 mV. For the study of Cr poisoning, LSCF cathodes were also examined in the presence of a Fe-Cr alloy interconnect under the open circuit condition at 800 and 900 ^{o}C for 20 h. The electrode was stabilized in air for 1 h before the electrochemical measurement. The EIS spectra were fitted using equivalent circuits as shown in Figure S2, which are composed of an inductance, L, resulting from the instrumentation, a resistor R_{Ω} for the ohmic resistance and a series of RQ elements (a resistor R_n in parallel with a constant phase element CPE_n) taking into account possible processes including electrode/electrolyte interfacial charge transfer resistance, oxygen surface exchange and solid state diffusion, as well as gas phase diffusion. The attribution of Rn to different physical processes is given in the results and discussion section below. The electrode total polarization resistance (R_p) is characterized by the addition of individual R_n.

2.3 Microstructure characterization

2.3.1 Characterization of bulk samples

Characterization of the bulk sample was carried out using scanning electron microscopy (SEM, LEO Gemini 1525 equipped with an energy-dispersive X-ray spectroscopy (EDX) detector) and X-ray diffraction (XRD, Bruker D8 Advance diffractometer using Cu-Kα radiation in the 2θ range 20°- 80°, with a step size of 0.0334° and a count time at each step of 1 s). Focused Ion Beam Scanning Electron Microscopy (FIB-SEM) was carried out using a dual beam system (Zeiss Auriga FIB-SEM, 30kV, 100 pA – 10 nA) to obtain morphology of the cross-sectional surface at particular locations for better understanding of the Cr distribution.

2.3.2 TEM analysis

TEM analysis of the cathode structure and chemistry was carried out on a JEOL 2100F microscope operating at 200 kV equipped with an 80 mm silicon drift EDX detector and a Gatan Tridiem imaging filter for EELS, a FEI Titan™ 80-300 microscope operated at 300 kV equipped with a field emission electron gun, a monochromator, a Cs-image corrector and Gatan Tridiem 866 imaging filter. Post-processing X-ray analysis was performed using Aztec (Oxford Instruments, UK) and Esprit (Bruker Nano GmbH, Berlin, Germany). The STEM probe size used for EDX mapping

was between 0.15-0.5 nm and the EELS energy resolution was varied between 0.8 and 2 eV depending on the experimental conditions used, defined as the full width at half-maximum of the zero-loss peak (ZLP). TEM foils were prepared from the LSCF porous layer by FIB milling using a Helios NanoLab 600 instrument (2-30 keV Ga^+ incident beam energy with currents of 16 pA - 21nA). To facilitate the preparation from the very porous structure, the samples were first infiltrated with a commercial embedding resin (Epon_812 substitute, MNA, DDSA and DMP, Sigma-Aldrich Co. LLC, Dorset, UK). TEM specimens were FIB polished at the last stage with 5 keV and then 2 keV Ga^+ beam to reduce the damage caused by the high energy Ga^+ beam.

3. Results and discussion

3.1 Electrochemical properties

Representative impedance spectra of the reference and degraded cells are shown in Figure 1 and the fitting results are shown in Table 1. It was found that the starting resistance of the cell at 0 hour varies slightly between samples measured at the same temperature, so the change of the cathode performance during the poisoning was characterized by following the change of the same cell. Based on the calculated capacitance C_n from the fitting results, the individual R_n can be attributed to different physical processes. The high frequency component with a capacitance C in the order of 10^{-4} to 10^{-5} F/cm^2 is in good agreement with the reported C values associated with the charge (oxygen ions) transfer resistance (R_1, R_{ct}) at the electrode/electrolyte interface for model LSCF cathodes with CGO or yttrium stabilized zirconia (YSZ) electrolytes [27, 28]. The intermediate frequency component with a capacitance C of 10^{-1} to 10^{-3} F/cm^2 is typically attributed to the electrochemical resistance (R_{chem}) of mixed ionic electronic conducting (MIEC) cathodes involving non-charge transfer processes including the oxygen surface reaction and the solid-state diffusion of oxygen [29, 30]. A small low frequency contribution associated with a capacitance between 1 and 10 F/cm^2 is sometimes identified at 900 ^{o}C. Such a large capacitance is unlikely to be from any electrochemical process and is attributed to the gas phase diffusion process above or in the cathode [31]. The results show that before Cr poisoning R_p at 800 ^{o}C is typically composed of R_{ct} and R_{chem} while at 900 ^{o}C only R_{chem} dominates with a small contribution of the gas phase diffusion resistance R_{gas}. In agreement with the previous study [28], R_{ct} is seen to have a strong dependence on the temperature, decreasing sharply with increasing temperature.

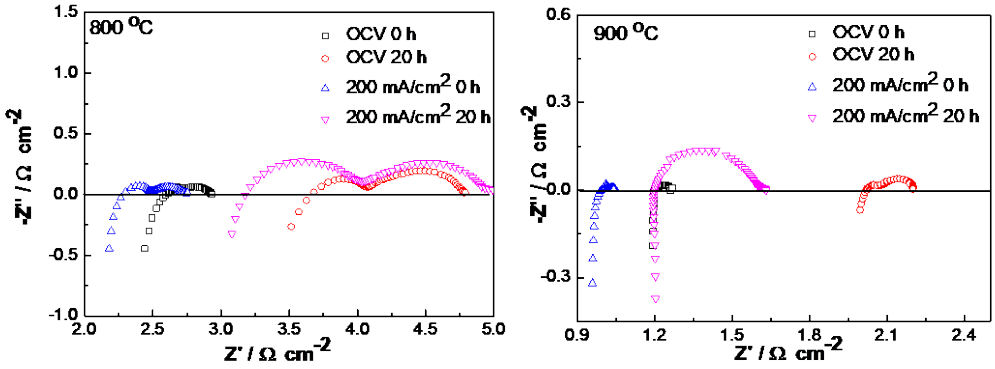

Figure 1 Representative EIS data of the cells before poisoning and poisoned under (a) OCV or (b) a constant cathodic current density of 200 mA cm^{-2} for 20 hours at 800 and 900 °C.

Table 1 Fitted impedance parameters showing ohmic resistance R_Ω, charge transfer resistance R_{ct}, electrochemical resistance R_{chem}), gas phase diffusion resistance R_{gas}, total polarization resistance R_p (R_{ct} + R_{chem} + R_{gas}) and their change after poisoning.

R (Ω cm^2) C (F/cm_2)	800°C				900°C			
	OCV		Pol.		OCV		Pol.	
	0 h	20 h	0 h	20 h	0 h	20 h	0 h	20 h
R_Ω	2.45	3.21	2.14	2.88	1.19	1.95	1.36	2.05
R_1 (R_{ct})	0.20	0.98	0.34	1.18	0	0.12	0	0
C_1 (C_{ct}) (X 10^{-5})	2.60	6.16	2.18	1.02	0	3.49	0	0
R_2 (R_{chem})	0.30	0.74	0.26	0.91	0.03	0.13	0.12	0.27
C_2 (C_{chem})	0.04	0.03	0.10	0.04	0.10	0.08	0.02	0.02
R_3 (R_{gas})	0	0	0	0	0.04	0	0	0.03
C_3 (C_{gas})	0	0	0	0	1.63	0	0	2.37
R_p (R_1+R_2+R_3)	0.5	1.72	0.6	2.09	0.07	0.25	0.12	0.30
$R_{ct,Cr}/R_{ct,\ ref}$	-	4.90	-	3.47	-	greatly increased	-	-
$R_{chem,Cr}/R_{chem,\ ref}$	-	2.47	-	3.50	-	4.33	-	2.25
$R_{p,Cr}/R_{p,\ ref}$	-	3.44	-	3.48	-	3.57	-	2.50

As expected, after 20 hours operation of the cell in the presence of the Cr alloy interconnect, the total electrode polarization resistance R_p increased by a factor of ~3 (Table 1). Comparing the OCV and the polarization conditions, at 800 °C, no obvious difference on the increase in R_p was found within the relatively short period of 20 hours; at 900 °C the increase of R_p was higher under OCV, which qualitatively agrees with the observation reported by Konysheva [25], who showed that the application of current led to three times slower degradation in R_p after 1000 hours poisoning of a LSCF cathode/CGO barrier layer/YSZ electrolyte/Pt electrode half-cell at 900 °C. When the different contributions of the individual resistances to R_p is analysed, some additional interesting observations related to the effect of polarization can be summarized as below: (1) R_{ct} increased significantly under OCV more than with the application of current, especially at 900 °C. (2) The small gas phase diffusion resistance seen for 900 °C remains negligible after poisoning. (3) Most interestingly, the temperature and polarization exhibit a synergistic effect. With the cathodic polarization, the increase of R_{chem} was higher than that under OCV at 800 °C but much less at 900 °C.

3.2 Cr incorporation at the micrometre scale

At the micrometre level, the incorporation of Cr species is most evidently present as Cr rich deposits at the surface (Figure 2a and b). EDX analysis confirmed that the deposits contain mainly Sr and O in addition to Cr, suggesting that it is the commonly reported $SrCrO_4$ phase, in agreement with the XRD patterns shown in Figure S3. The amount of $SrCrO_4$ deposit *at the surface* is significantly higher at 900 °C than at 800 °C and is much more pronounced at the rib position where a direct contact between the interconnect and the cathode was made. At 900 °C, the surface deposition of $SrCrO_4$ at the rib position forms a continuous layer as shown in the cross-sectional surface revealed by FIB, which has a similar thickness of ~2 µm under both OCV and polarization conditions (Figure 2c). The presence of current passage did not appear to have a significant effect on the amount of $SrCrO_4$ deposits at the surface at both temperatures, which supports the theory that the $SrCrO_4$ *surface deposition* has a nature of chemical reaction and is enhanced by higher temperatures and solid-state diffusion [12].

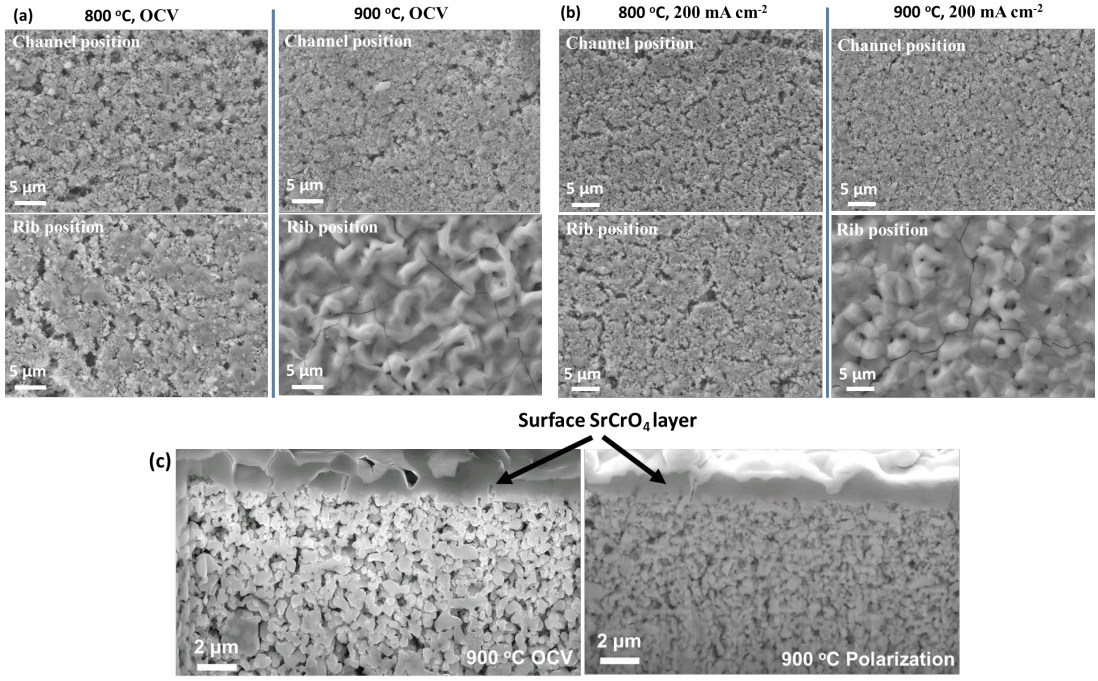

Figure 2 Microstructure and morphology of the LSCF4628 cathode layer after poisoning at 800 and 900 °C. (a) Surface of the cathode poisoned for 20 h under OCV. (b) Surface of the cathode poisoned for 20 h with a cathodic polarization of 200 mA cm^{-2}. (c) Comparison of the cathode cross-section revealing the thickness of $SrCrO_4$ surface deposit for samples poisoned at 900 °C with/without polarization.

EDX was performed on the FIB prepared cross-sectional surface of the cathode layer to investigate the Cr distribution *inside the cathode* up to the cathode/electrolyte interface. The average Cr content inside the cathode was estimated by area EDX analysis from the cross-sectional surface. Areas with a ~20 µm width and a depth from just below the surface $SrCrO_4$ layer to the cathode/electrolyte interface were selected. The results are shown in Table 2. The bulk Cr level was consistently higher at 900 °C compared to that at 800 °C, and higher in the location below the rib than the channel, similar to what was observed for the surface Cr deposit. However, comparing the samples poisoned under different polarization conditions, it is interesting to see that the at 900 °C the reduced

poisoning effect under the polarization condition corresponds to a higher Cr content compared to the OCV condition. The results therefore confirm that more Cr incorporation is not necessarily associated with enhanced cathode degradation.

Table 2 Average Cr contents inside the cathode for different poisoned samples*

Cr content (at. %)	800 °C		900 °C	
	OCV	with polarization	OCV	with polarization
Below Rib	3.8 ± 0.3	4.6 ± 1.0	3.0 ± 0.8	9.1 ± 0.6
Below Channel	0.4 ± 0.2	1.4 ± 0.2	1.3 ± 0.6	2.6 ± 0.4

* The indicated error of the Cr content only includes the statistical deviation obtained from multiple measurements. The relative comparison of the Cr content here is reliable as all the EDX data acquisition and quantification were performed under the same experimental conditions using the same quantification parameters. Please refer to the supplementary information including Figure S4 and Table S1 for more information.

As the average Cr content only indicates the level of total Cr incorporation, SEM-EDX elemental mapping was performed as an attempt to investigate the type and distribution of Cr phases (Figure 3 and S2). Some differences can be noted between the samples poisoned with and without polarization at 900 °C. For the OCV sample, Cr incorporation was found to be present as the $SrCrO_4$ phase at the surface and close to the cathode/electrolyte interface. Meanwhile, a large amount of Co segregation can be seen clearly, which is expected to be the $FeCoO_x$ spinel as reported in our earlier work [15]. For the polarized sample, it can be seen that in addition to $SrCrO_4$ there are obvious regions where the enrichment of Cr coincides with that of Co, instead of Sr. For samples poisoned at 800 °C, the $SrCrO_4$ phase and Co rich precipitates were similarly present inside the cathode, but the amount of both phases is lower than at 900 °C. This is expected as thermodynamically the vapour pressure of CrO_3 and the decomposition of LSCF is reduced at lower temperatures [32, 33]. The co-enrichment of Cr and Co is not evident at 800 °C at the SEM resolution (Figure S5).

The embedded LSCF/CGO interfaces of the cells poisoned at 900 °C were examined from the cross-sectional surface revealed by FIB milling, which was intended to avoid possible artefacts on the interface adhesion due to a cutting, grinding and polishing procedure. As shown in Figure 4, while the interface of the sample poisoned under polarization maintains good adhesion between LSCF and CGO, the one under OCV exhibits severe delamination, which could be responsible for the observed large increase in the interfacial charge transfer resistance after poisoning.

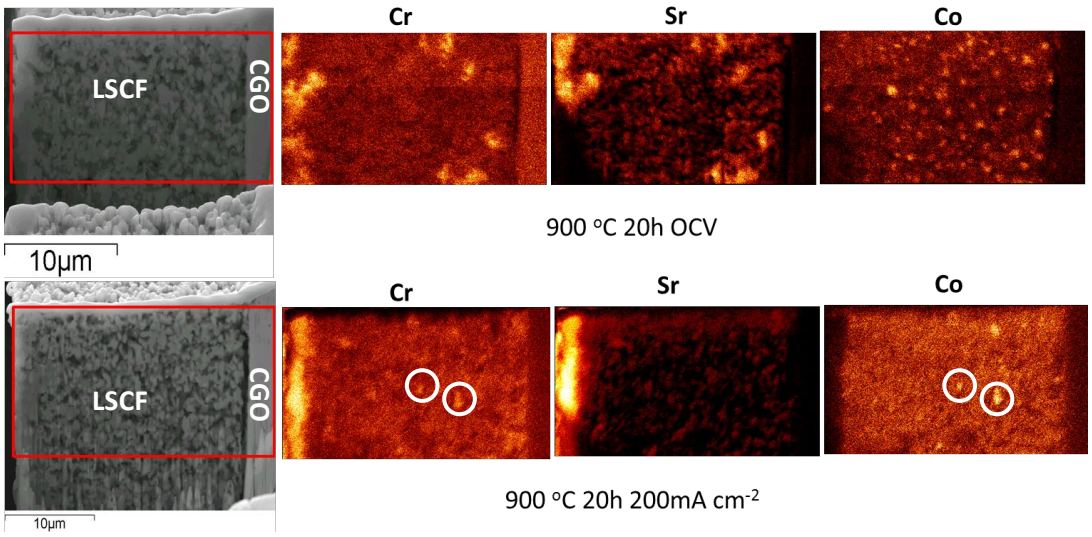

Figure 3 EDX map of the cross-section surface of the LSCF cathode layer for samples poisoned at 900 °C. Some Cr and Co rich locations are circled for the sample poisoned with the current passage. The low intensity shown in the bottom left corner of the elemental maps is due to the shadowing effect introduced by the position of the EDX detector in the FIB instrument.

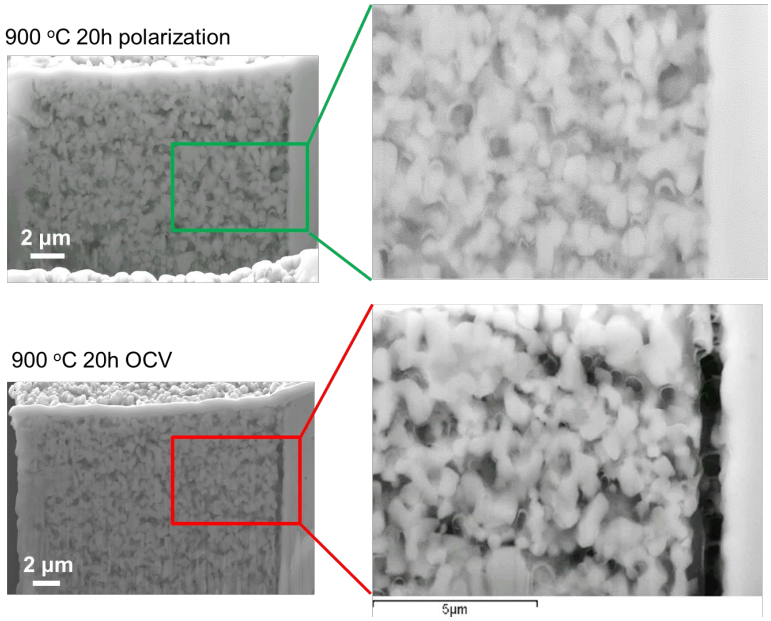

Figure 4 The LSCF/CGO interface in the sample poisoned at 900 °C for 20 hours. (a) OCV (b) with a cathodic polarization of 200 mA cm^{-2}

3.3 Cr incorporation at the nanometre scale

In order to further elucidate the Cr incorporation behaviour into the cathode layer, careful TEM experiments were carried out on all the poisoned samples focusing on the Cr distribution inside the LSCF cathodes down to the cathode/electrolyte interface. In the interest of conciseness, the large body of TEM results will be summarized into two parts: (1) Cr incorporation behaviour common to all the samples and (2) differences that were observed for the sample poisoned at 900 °C with polarization.

3.3.1 Cr incorporation behaviour common to all the samples

The most obvious observation in the cathodes after poisoning was the formation of $SrCrO_4$ and FeCoOx spinel phases, confirmed by STEM-EDX mapping and electron diffraction, in agreement with the results previously identified for the model system (LSCF cathodes in symmetric cells poisoned with direct infiltration of Cr solution) [15]. A representative STEM EDX mapping is shown in Figure 5a. Figure 5b shows clearly the formation of $SrCrO_4$ phase by consuming Sr in the adjacent LSCF grain. The amount of $SrCrO_4$ and $FeCoO_x$ phases inside the cathode is in general lower at 800 °C compared to 900 °C, consistent with the SEM-EDX results. The amount of $FeCoO_x$ spinel increased consistently with that of $SrCrO_4$, confirming the enhanced B site element precipitation upon the loss of Sr in LSCF due to the formation of $SrCrO_4$ [15]. Figure 6 represents the correlation between the formation of phases of $SrCrO_4$, $FeCoO_x$ and LSCF depleted in Co and Fe.

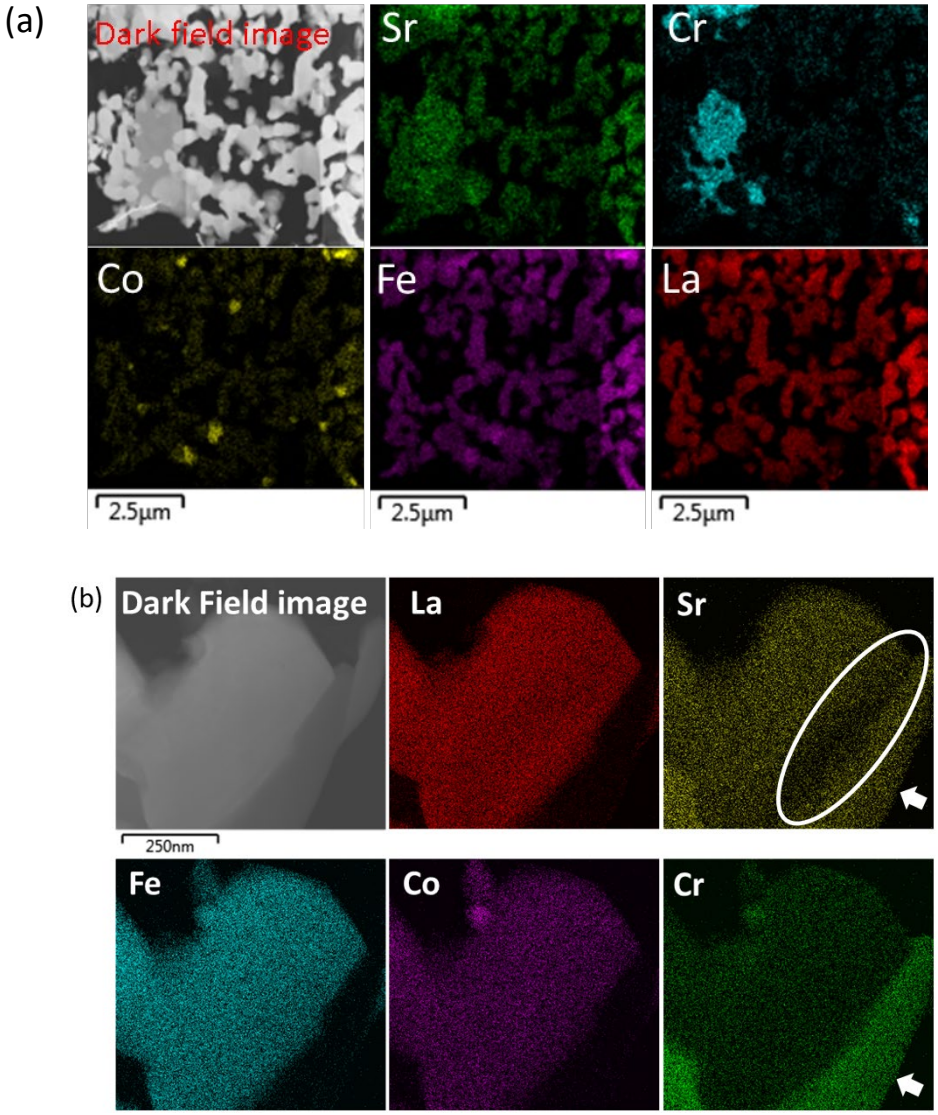

Figure 5 (a) Representative STEM-EDX mapping showing the typical formation of $SrCrO_4$ and $FeCoO_x$ phases. (b) Growth of the $SrCrO_4$ grain (arrowed) by consuming Sr in the adjacent LSCF grain (circled).

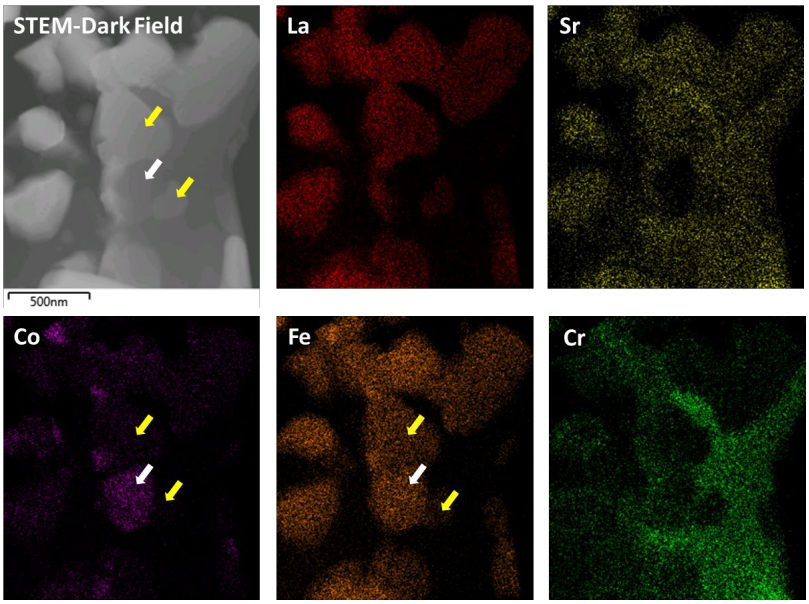

Figure 6 STEM-EDX mapping showing the correlation between the $SrCrO_4$ phase, the LSCF grain depleted in Fe and/or Co (yellow arrow) and the adjacent $FeCoO_x$ precipitate (white arrow).

Grain boundary segregation of Cr (Figure S6) was also observed for all the samples and Cr substitution into the B site of LSCF (Figure 7) was identified mainly in the cathodes poisoned at 900 °C. The observations confirm that these two Cr poisoning mechanisms, as discovered in our previous study for the model system where the poisoning was carried out by direct infiltration of Cr containing solutions into the cathodes [15], also occur in the more realistic poisoning conditions used in the current study. The representative example shown in Figure 7 clearly indicates the substitution started at the grain surface and gradually proceeded to the grain interior. The simultaneous depletion of Co is also evident, confirming the preferential substitution of Co, as found in our previous study [15].

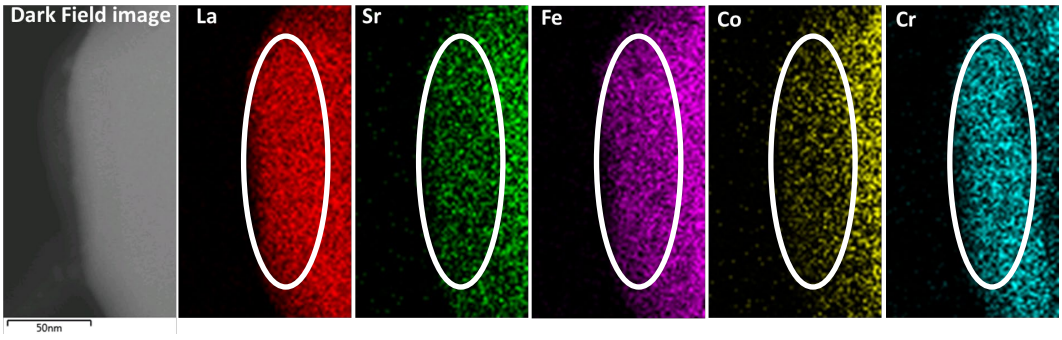

Figure 7 STEM-EDX mapping of the edge of a LSCF grain, showing the Cr substitution starting from the grain surface

3.3.2 Cr incorporation behaviour in the cathode poisoned at 900 °C with cathodic polarization

Detailed TEM experiments revealed some distinct features on the Cr incorporation behaviour exclusively for the cathode poisoned at 900 °C with the passage of 200 mA cm^{-2} cathodic current. While $SrCrO_4$ was the main phase formed at the cathode surface, inside the cathode Cr was frequently found to be present in association with Co, Fe, O in addition to $SrCrO_4$, as evidenced in Figure 8a. EDX quantification using pristine LSCF and $SrCrO_4$ formed in poisoned samples as the standards suggested a composition of $FeCoCr_2O_x$ and electron micro-diffraction identified

a spinel structure with a ~ 8.33 Å, similar to the $FeCoO_x$ phase (Figure 8b). An epitaxial relationship was observed between the $FeCoCr_2O_x$ phase and the adjacent LSCF grain, indicating the exsolution of Co and Fe from the parent LSCF (Figure S7).

The formation of this Cr rich spinel phase was found to be present throughout the cathode up to the cathode/CGO interface. More interestingly, a thin layer deposition with a composition of ~ $FeCoCr_2O_x$ was identified at the surface of the CGO electrolyte (Figure 9). TEM investigation confirmed that $FeCoCr_2O_x$ formation is not significant at 800 ^oC under polarization. It is also noted that occasionally this phase was observed in samples poisoned under other conditions, however its amount was very low and the $SrCrO_4$ phase was always the predominant Cr containing product.

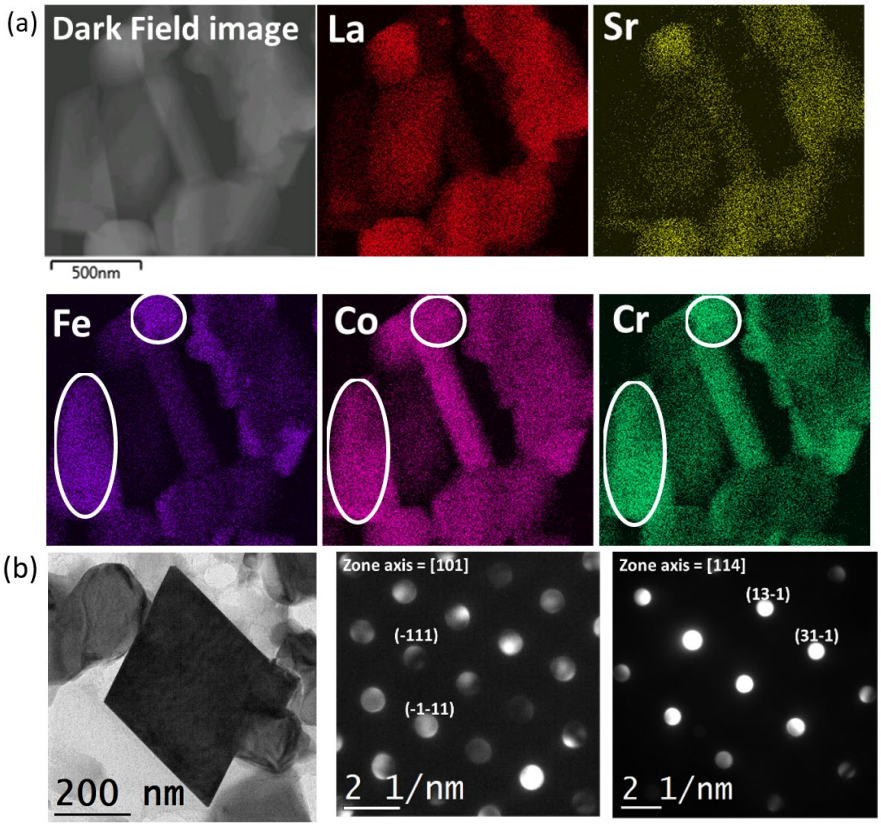

Figure 8 (a) Representative STEM-EDX mapping showing the presence of $FeCoCr_2O_x$ (circled) grains in the sample poisoned at 900 ^oC with the passage of 200 mA cm^{-2} cathodic current. (b) Bright field TEM image of a representative $FeCoCr_2O_x$ phase showing better its morphology and the corresponding electron diffraction patterns taken at two different zones confirming its spinel structure.

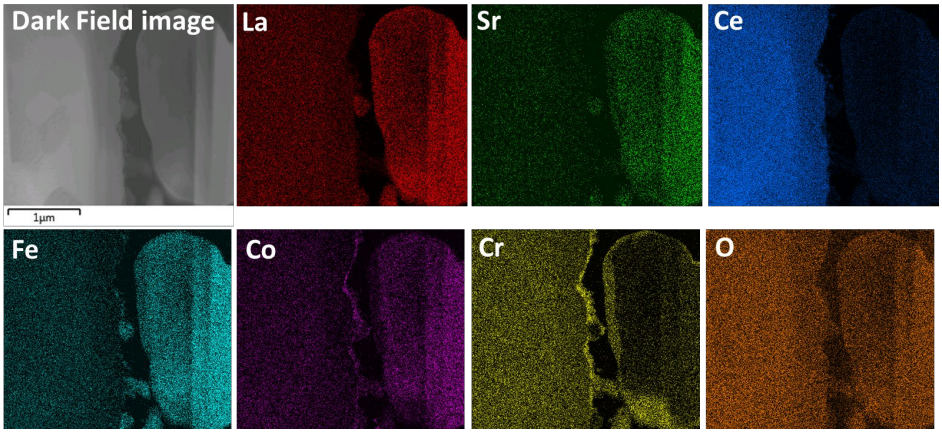

Figure 9 STEM-EDX mapping showing the deposition of $FeCoCr_2O_x$ phase at the cathode/CGO interface.

3.4. Cr poisoning mechanisms

Overall, the following Cr incorporation modes have been identified in the current work:

a. Formation of $SrCrO_4$

b. Segregation of Cr into grain boundaries, which is associated with depletion of Co

c. Substitution of Cr in the B site of LSCF lattice

d. Enhanced formation of $FeCoO_x$ spinel (not shown in this work, but known from our previous investigation [15])

e. Formation of $FeCoCr_2O_x$ spinel

The significance of these modes for different samples is summarized in Table 3.

Table 3. Modes of Cr incorporation in the LSCF cathode under different temperature and polarization conditions.

Mechanisms	**800 °C OCV**	**800 °C 200 mA cm^{-2}**	**900 °C OCV**	**900 °C 200 mA cm^{-2}**
$SrCrO_4$ formation	Cathode surface and interior	Cathode surface and interior	Cathode surface and interior	Cathode surface and interior
	Greatly enhanced at 900 °C compared to 800 °C			
Cr substitution in LSCF	Negligible	Negligible	Observed	Observed
Cr GB segregation	Observed	Observed	Observed	Observed
$FeCoO_x$ formation	Observed	Observed	Observed	Observed
$FeCoCr_2O_x$ formation	Negligible	Negligible	Negligible	Large amount, distributed

We will now focus on the discussion of the mechanisms that led to the observed poisoning effect on the cathode under different conditions, as described in Section 3.1 and Table 3. The formation of the large surface $SrCrO_4$ deposit has been considered to be a major contribution to the deterioration of cathode performance [34, 35]. The current work however suggests that the *surface* $SrCrO_4$ may only increase the ohmic resistance at the cathode/interconnects contact while having a minor effect on the electrochemical properties of the cathode. This is because between the samples poisoned at 900 °C with and without polarization, which exhibited a significant

difference in terms of the increase of R_{chem} upon poisoning, the thickness and morphology of surface $SrCrO_4$ was very similar. Although significant surface $SrCrO_4$ was identified at 900 °C after poisoning, negligible gas diffusion resistance was measured, which indicates that the access of oxygen to the cathode inner surface was not limited. This is actually not very surprising as the large amount of surface $SrCrO_4$ is mainly located at the rib position, where oxygen gas transport would be expected to be negligible in the first place.

Moving on to the Cr incorporation modes observed *inside the cathode*, current work confirms that all the mechanisms previously identified in a model system (i.e. introduction of Cr source by directly infiltrating Cr solution into LSCF cathodes of symmetrical cells [15]) are also present in the more realistic poisoning condition (i.e. introduction of Cr source by using Cr containing metallic interconnects and cell operation under polarization). By comparing different poisoning temperatures, it can be concluded that a higher temperature promotes the poisoning effect, which is associated with increased $SrCrO_4$ formation and Cr substitution of Fe and Co at the B site of LSCF at 900 °C compared with 800 °C. While the former mechanism is known from many previous studies including ours (e.g. ref. 35 and 21), the Cr substitution behaviour was only recently identified in our previous work [15]. In the current work, we identified experimental evidence of significant Cr substitution only at a high temperature of 900 °C, in agreement with a favoured Cr substitution with increasing temperatures as predicted by thermodynamic calculations [36]. The Cr segregation into the grain boundary was observed at both temperatures, indicating grain boundary diffusion of Cr is much faster than its lattice diffusion, as measured by Wærnhus et al [37]. Due to the limited number of grain boundaries that was suitable for TEM characterization, it was difficult to quantitatively compare the level of grain boundary segregation between 800 and 900 °C, although thermodynamically this should also be enhanced at 900 °C.

Comparing the poisoning under different polarization conditions, it was found that at 800 °C polarization degraded R_{chem} more, corresponding to a higher amount of Cr within the cathode in the format of $SrCrO_4$, substitution in LSCF and segregation at grain boundaries. This appears to suggest that Cr incorporation *inside the cathode* does involve electrochemical reduction of Cr(VI). Most interestingly, the correlated EIS and multiscale microstructural analysis reveals that the reduced degradation of R_{chem} at 900 °C with polarization was not consistent with the highest amount of incorporated Cr, but associated with a different Cr incorporation mode, i.e. the significant formation of $FeCoCr_2O_x$ inside the cathode up to the cathode/electrolyte interface. Firstly, the enhanced Cr level might be related to the additional $FeCoCr_2O_x$ phase acting as an extra Cr getter as indicated in the following reactions (Equation 1 and 2):

$$(La_{0.6}Sr_{0.4})(Co_{0.2}Fe_{0.8})O_3 + 0.8CrO_3 \rightarrow 0.4SrCrO_4 + 0.6LaFeO_3 + 0.2FeCoCr_2O_x \quad \text{(Eq. 1)}$$

$$(La_{0.6}Sr_{0.4})(Co_{0.2}Fe_{0.8})O_3 + 0.4CrO_3 \rightarrow 0.4SrCrO_4 + 0.6LaFeO_3 + 0.2FeCoO_x \quad \text{(Eq. 2)}$$

Secondly, the effect of preferential $FeCoCr_2O_x$ formation with respect to $SrCrO_4$ appears to be beneficial in terms of poisoning resistance, which can be discussed in the following aspects: (1) In terms of the electrical conductivity, $SrCrO_4$ was reported to have a DC conductivity of $1.8x10^{-4}$ Ω cm^{-1} at 800 °C [38] while a value of $2.9x10^{-3}$ Ω cm^{-1} at 800 °C was estimated for a Cr substituted cobalt ferrite $CoFe_{1.6}Cr_{0.4}O_4$ [39], therefore it can be expected that the conductivity of $FeCoCr_2O_x$ is slightly higher than that of $SrCrO_4$; (2) as a type of ferrite spinel the $FeCoCr_2O_x$ is considered to have a potential in catalysis applications [40]. The complementary micro- and nanoscale analysis (Figure 4 and 9) reveals that the $SrCrO_4$ phase was present mainly as larger but fewer grains (up to several microns) while the $FeCoCr_2O_x$ tended to form finer but larger number of particles (200-500 nm) that were distributed more homogeneously within the cathode. More critically, $FeCoCr_2O_x$ type of phase was found to directly coat the CGO surface at the cathode/electrolyte interface (Figure 9). As a result, the effective electrochemically active area, especially within electrode utilization region thickness, δ (typically several um according to literature [10, 41] for the MIEC cathode), is expected to significantly increase with the formation of a large amount of fine $FeCoCr_2O_x$. The difference in the morphology between $FeCoCr_2O_x$ and $SrCrO_4$ is likely to be the result of Fe and Co being more mobile than SrO, which are the precursors for the two phases respectively. In the light of many previous researches that has achieved better LSCF performance and Cr tolerance by the application of a conformal catalyst coating on the cathode such as $Pr_{0.75}Ca_{0.2}MnO_{3-\delta}$ and $Pr_{0.8}Ca_{0.2}FeO_{3-\delta}$ [23], the insitu formation of $FeCoCr_2O_x$ can be an effective alternative way for enhancing the Cr resistance and electrochemical property of LSCF cathodes.

The observation that under the OCV condition Cr preferentially reacts with Sr instead of the B site elements of LSCF (e.g. Co) is consistent with previous studies e.g. ref. 5. The additional interaction mode leading to the formation of $FeCoCr2O_x$ under cathodic polarization is a new phenomenon that has not been revealed before, although a similar phase of $(Fe,Cr)_2O_3$ was found when directly heating a mixed powder of LSCF and Cr_2O_3 at 800 oC for long time (~100 h) [42]. The main driving force for the spinel formation can be interpreted as a facilitated electrochemical reduction of Cr (VI), and/or a reduced local oxygen partial pressure in the LSCF cathode with the applied polarization, which favours Cr (III) in the spinel over Cr (VI) in $SrCrO_4$. The expected valence state of Cr in $FeCoCr_2O_x$ with respective to that in $SrCrO_4$ was also confirmed by EELS fine structure as shown in Figure S8. The Cr-L3 edge maximum from $SrCrO_4$ particles is ~ 580 eV with a low energy shoulder and that from $FeCoCr_2O_x$ is ~ 577 eV, in good agreement with what has been reported for Cr 6+ and Cr 3+ respectively [43]. It is noted that at 800 °C the polarization effect is smaller and the $FeCoCr_2O_x$ formation is not significant, suggesting that the relative stability of $SrCrO_4$ over $FeCoCr_2O_x$ is higher at lower temperatures.

5. Conclusions

LSCF cathodes in a LSCF/CGO/Pt half cell were poisoned by Cr at different temperatures and polarization conditions with a Cr-Fe alloy as the interconnect. Cr induced degradation as a function of temperature and polarization conditions was analysed by EIS focusing on R_{chem} that reflects the cathode electrochemical properties. It was found that R_{chem} increased more with increasing temperatures and with polarization at 800 ^{o}C. However, at 900 ^{o}C polarization reduced the increase in R_{chem}, i.e. the degradation in the electrochemical property of the LSCF. It is noticed that if only the total polarization R_{pol} was considered, the distinct effect of polarization would not be evident. The results therefore point out that a detailed EIS analysis is preferred to reveal the poisoning effect on individual degradation processes.

By correlating complementary micro- and nano-scale microstructure characterization with impedance analysis, the degradation mechanisms were investigated and can be summarized as the following:

1) Apart from the well-known $SrCrO_4$ formation, several new nanoscale mechanisms of Cr incorporation identified previously for model systems, including Cr grain boundary segregation, Cr substitution in LSCF leading to enhanced $FeCoO_x$ spinel formation [15], were confirmed in the current system, which resembles more closely practical SOFC operation and Cr poisoning situations.

2) The electrochemical degradation in terms of R_{chem} was found not to correlate with the amount of *surface $SrCrO_4$ deposits* but with a synergistic effect coupling the amount and the modes of Cr incorporation *inside the cathode* as a function of temperature and polarization conditions. Higher temperatures promoted the decomposition of LSCF and Cr diffusion, leading to enhanced formation of $SrCrO_4$, Cr substitution in the perovskite LSCF and segregation to grain boundaries, finally a higher poisoning effect. The cathodic polarization had different effects depending on the temperature. At 800 ^{o}C polarization increased the amount of Cr incorporated inside the cathode, leading to a greater increase in R_{chem}. However at 900 ^{o}C cathodic polarization reduced the poisoning effect although the measured Cr content inside the cathode was higher than that under the OCV condition. The beneficial effect can be attributed to the formation of the $FeCoCr_2O_x$ phase, which were present as fine particles of 200-500 nm distributed uniformly across the cathode thickness up to the cathode/electrolyte interface. The spinel phase has been previously reported to have a potential in catalysis applications and could enhance the cathode electrochemical property.

3) The passage of current appears to have helped preventing delamination of the cathode/electrolyte interface thus reducing the charge transfer resistance.

4) The overall results also suggest that both direct chemical reaction of Cr species with LSCF and electrochemical reduction of Cr (VI) are active Cr incorporation mechanisms. The former was responsible for the deposition of

$SrCrO_4$ *at the cathode surface*, while the latter was involved in the formation of $SrCrO_4$ and $FeCoCr_2O_x$ phases *inside the cathode*.

Previous studies of Cr poisoning of Sr containing perovskite cathodes have long focused on the undesirable instability of Sr. The new mechanisms identified in the current study reveals that the activity of B site elements in LSCF and possible other perovskite cathodes can have a positive effect under certain combined temperature and polarization conditions, therefore future research in designing Cr resistant perovskite cathode materials may consider strategies that utilize the exsolution of B site elements for the formation of beneficial spinel phases. More generally, the insitu formation of spinel phases could be an approach for material optimization in similar electrochemical applications such as solid oxide electrolysis cells using perovskite ceramic electrodes.

Conflicts of interest

There are no conflicts to declare.

Acknowledgement

This work has been supported by Shanghai Pujiang Program (No. 18PJ1406500), Imperial College London Research Fellowship, Australia Research Council (DP180100731) and 2019 Youth Innovative Talents Project by Education Department of Guangdong Province.

References

1. M. Liu, D. Ding, K. Blinn, X. Li, L. Nie and M. Liu, *International Journal of Hydrogen Energy*, 2012, **37**, 8613-8620.
2. A. Esquirol, N. P. Brandon, J. A. Kilner and M. Mogensen, *Journal of The Electrochemical Society*, 2004, **151**, A1847-A1855.
3. C. Sun, R. Hui and J. Roller, *J Solid State Electrochem*, 2010, **14**, 1125-1144.
4. D. Oh, D. Gostovic and E. D. Wachsman, *Journal of Materials Research*, 2012, **27**, 1992-1999.
5. L. Zhao, J. Drennan, C. Kong, S. Amarasinghe and S. P. Jiang, *Journal of Materials Chemistry A*, 2014, DOI: 10.1039/c1034ta01426j.
6. S. P. Simner, M. D. Anderson, M. H. Engelhard and J. W. Stevenson, *Electrochemical and Solid-State Letters*, 2006, **9**, A478-A481.
7. Z. B. Yang, M. Y. Guo, N. Wang, C. Y. Ma, J. L. Wang and M. F. Han, *International Journal of Hydrogen Energy*, 2017, **42**, 24948-24959.
8. K. Min, C. W. Sun, W. Qu, X. G. Zhang, S. Yick, M. Robertson, C. Decès-Petit and R. Hui, *International Journal of Green Energy*, 2009, **6**, 627-637.
9. S. P. Jiang and X. B. Chen, *International Journal of Hydrogen Energy*, 2014, **39**, 505-531.
10. Y. Huan, Y. Fan, Y. Li, B. Yin and T. Wei, *Journal of Materials Chemistry A*, 2018, **6**, 5172-5184.
11. S. P. Jiang, *Solid State Ionics*, 2002, **146**, 1-22.
12. S. P. Jiang, S. Zhang and Y. D. Zhen, *Journal of the Electrochemical Society*, 2006, **153**, A127-A134.
13. L. Zhao, J. Zhang, T. Becker and S. P. Jiang, *Journal of the Electrochemical Society*, 2014, **161**, F687-F693.

14. L. Zhao, J. Drennan, C. Kong, S. Amarasinghe and S. P. Jiang, *Journal of Materials Chemistry A*, 2014, **2**, 11114-11123.
15. N. Ni, S. J. Cooper, R. Williams, N. Kemen, D. W. McComb and S. J. Skinner, *ACS Applied Materials & Interfaces*, 2016, **8**, 17360-17370.
16. S. P. Jiang, J. P. Zhang, L. Apateanu and K. Foger, *Journal of The Electrochemical Society*, 2000, **147**, 4013-4022.
17. M. Krumpelt, T. A. Cruse, B. J. Ingram, J. L. Routbort, S. Wang, P. A. Salvador and G. Chen, *Journal of The Electrochemical Society*, 2010, **157**, B228-B233.
18. S. Taniguchi, M. Kadowaki, H. Kawamura, T. Yasuo, Y. Akiyama, Y. Miyake and T. Saitoh, *Journal of Power Sources*, 1995, **55**, 73-79.
19. S. P. S. Badwal, R. Deller, K. Foger, Y. Ramprakash and J. P. Zhang, *Solid State Ionics*, 1997, **99**, 297-310.
20. E. Konysheva, J. Mertens, H. Penkalla, L. Singheiser and K. Hilpert, *Journal of The Electrochemical Society*, 2007, **154**, B1252-B1264.
21. C. C. Wang, T. Becker, K. Chen, L. Zhao, B. Wei and S. P. Jiang, *Electrochimica Acta*, 2014, **139**, 173-179.
22. S. P. Jiang, J. P. Zhang and X. G. Zheng, *Journal of the European Ceramic Society*, 2002, **22**, 361-373.
23. Y. Chen, S. Yoo, X. Li, D. Ding, K. Pei, D. Chen, Y. Ding, B. Zhao, R. Murphy, B. deGlee, J. Liu and M. Liu, *Nano Energy*, 2018, **47**, 474-480.
24. J. J. Bentzen, J. V. T. Høgh, R. Barfod and A. Hagen, *Fuel Cells*, 2009, **9**, 823-832.
25. E. Y. Konysheva, *Russian Journal of Electrochemistry*, 2014, **50**, 630-637.
26. S. P. Jiang and X. Chen, *International Journal of Hydrogen Energy*, 2014, **39**, 505-531.
27. J.-W. Lee, Z. Liu, L. Yang, H. Abernathy, S.-H. Choi, H.-E. Kim and M. Liu, *Journal of Power Sources*, 2009, **190**, 307-310.
28. F. S. Baumann, J. Fleig, H.-U. Habermeier and J. Maier, *Solid State Ionics*, 2006, **177**, 1071-1081.
29. R. Sayers, M. Rieu, P. Lenormand, F. Ansart, J. A. Kilner and S. J. Skinner, *Solid State Ionics*, 2011, **192**, 531-534.
30. K. Zhao, Q. Xu, D.-P. Huang, W. Chen, M. Chen and B.-H. Kim, *J Solid State Electrochem*, 2012, **16**, 9-16.
31. J. Nielsen, T. Jacobsen and M. Wandel, *Electrochimica Acta*, 2011, **56**, 7963-7974.
32. W. Zhang, M. Chen, P. V. Hendriksen and W.-R. Kiebach, *Journal*, 2014, 40-50.
33. K. Hilpert, D. Das, M. Miller, D. H. Peck and R. Weiß, *Journal of The Electrochemical Society*, 1996, **143**, 3642-3647.
34. F. Shen and K. Lu, *Electrochimica Acta*, 2016, **211**, 445-452.
35. B. Wei, K. Chen, C. C. Wang, Z. Lü and S. P. Jiang, *Solid State Ionics*, 2015, **281**, 29-37.
36. H. Yokokawa, T. Horita, N. Sakai, K. Yamaji, M. E. Brito, Y. P. Xiong and H. Kishimoto, *Solid State Ionics*, 2006, **177**, 3193-3198.
37. I. Wærnhus, N. Sakai, H. Yokokawa, T. Grande, M.-A. Einarsrud and K. Wiik, *Solid State Ionics*, 2007, **178**, 907-914.
38. W. Liu and E. Y. Konysheva, *ECS Transactions*, 2014, **59**, 327-332.
39. S. Supriya, S. Kumar and M. Kar, *Journal of Materials Science: Materials in Electronics*, 2017, **28**, 10652-10673.
40. K. O. Abdulwahab, M. A. Malik, P. O'Brien, I. J. Vitorica-Yrezabal, G. A. Timco, F. Tuna and R. E. P. Winpenny, *Dalton Transactions*, 2018, **47**, 376-381.
41. S. B. Adler, J. A. Lane and B. C. H. Steele, *Journal of The Electrochemical Society*, 1996, **143**, 3554-3564.
42. T. Komatsu, R. Chiba, H. Arai and K. Sato, *Journal of Power Sources*, 2008, **176**, 132-137.
43. T. L. Daulton and B. J. Little, *Ultramicroscopy*, 2006, **106**, 561-573.